European Journal of Pharmacology 912 (2021) 174584

Contents lists available at ScienceDirect

European Journal of Pharmacology

journal homepage: www.elsevier.com/locate/ejphar

Characterization of a high throughput human stem cell cardiomyocyte assay to predict drug-induced changes in clinical electrocardiogram parameters

Peter Kilfoil [a], Shuyun Lily Feng [a], Asser Bassyouni [a], Tiffany Lee [a], Derek Leishman [c], Dingzhou Li [b], David J. MacEwan [d], Parveen Sharma [e], Eric D. Watt [b], Stephen Jenkinson [a,*]

[a] Worldwide Research and Development, Pfizer Inc., La Jolla, CA, 92121, USA
[b] Groton, CT, 06340, USA
[c] Lilly Research Laboratories, Eli Lilly and Company, Indianapolis, IN, 46285, USA
[d] Department of Pharmacology and Therapeutics, Institute of Systems, Molecular and Integrative Biology, University of Liverpool, L69 3GE, UK
[e] Department of Cardiovascular & Metabolic Medicine, Institute of Life Course and Medical Sciences, University of Liverpool, L69 3GE, UK

ARTICLE INFO

Keywords:
Action potential
Clinical
QTc
Stem cell
Torsades de pointes

ABSTRACT

Human induced pluripotent stem cell derived cardiomyocytes (hIPSC-CM's) play an increasingly important role in the safety profiling of candidate drugs. For such models to have utility a clear understanding of clinical translation is required. In the present study we examined the ability of our hIPSC-CM model to predict the clinically observed effects of a diverse set of compounds on several electrocardiogram endpoints, including changes in QT and QRS intervals. To achieve this, compounds were profiled in a novel high throughput voltage-sensitive dye platform. Measurements were taken acutely (30 min) and chronically (24 h) to ensure that responses from compounds with slow onset kinetics or that affected surface ion channel expression would be captured. In addition, to avoid issues associated with changes in free drug levels due to protein binding, assays were run in serum free conditions. Changes in hIPSC-CM threshold APD_{90} values correlated with compound plasma exposures that produced a +10 ms change in clinical QTc (Pearson $r^2 = 0.80$). In addition, randomForest modeling showed high predictivity in defining TdP risk (AUROC value = 0.938). Risk associated with QRS prolongation correlated with an increase in action potential rise-time (AUROC value = 0.982). The in-depth understanding of the clinical translatability of our hIPSC-CM model positions this assay to play a key role in defining cardiac risk early in drug development. Moreover, the ability to perform longer term studies enables the detection of compounds that may not be highlighted by more acute assay formats, such as inhibitors of hERG trafficking.

1. Introduction

Development of in vitro assay systems that provide clinically translatable assessments of risk is a key goal within the pharmaceutical industry. One area receiving particular attention is the use of human induced pluripotent stem cell derived cardiomyocytes (hIPSC-CM) in defining cardiac safety (Gintant et al., 2020). hIPSC-CM express many prominent depolarizing and repolarizing ion channels that shape the action potential (AP) in the human heart (Zhao et al., 2018), as well as other components whose functions modulate the cellular membrane potential. As such, hIPSC-CM represent a promising platform for investigating the integrated effects of drugs on the cardiac AP. hIPSC-CM's, however, show an immature phenotype (Ivashchenko et al., 2013; Zhu et al., 2009) and consist of a mixed population of cardiac cell types (ventricular, atrial and nodal) (Ma et al., 2011). Hence although promising, the clinical translatability of such a cell system is still not fully defined.

Historically, in vitro safety profiling has heavily leveraged the testing of a compound's ability to block the human ether-a-go-go-related gene (hERG; $K_v11.1$) potassium channel when addressing a compound's impact on cardiac electrophysiology (Food and Drug Administration, 2005). Blockade of the hERG channel is associated with a delay in cellular repolarization that is observed as a prolongation of the QT of the electrocardiogram (ECG), resulting in the potential generation of

* Corresponding author. Pfizer Inc., 10646 Science Centre Drive, San Diego, CA, 92121, USA.
E-mail address: stephen.jenkinson@pfizer.com (S. Jenkinson).

https://doi.org/10.1016/j.ejphar.2021.174584
Received 20 August 2021; Received in revised form 12 October 2021; Accepted 18 October 2021
Available online 19 October 2021

cardiac arrythmias. hERG inhibition alone, however, may overestimate the proarrhythmic liability of a compound and prevent low risk candidate molecules from progressing through development (Johannesen et al., 2014). Such disconnects may arise when a compound blocks additional cardiac currents, particularly the inward L-type calcium ($I_{Ca,L}$) and sodium (I_{Na}) currents, that may balance hERG-mediated reduction in the repolarizing current. Thus, drugs that show mixed ion channel effects may maintain the delicate balance of outward and inward currents driving repolarization.

In recent years the FDA-supported Comprehensive In Vitro Proarrhythmia Assay (CiPA) project has aimed to develop clinically translatable assays to predict arrhythmia generation (Colatsky et al., 2016; Fermini et al., 2016). One pillar of this approach has focused on hIPSC-CM assays, and a wide array of methodologies have been examine, with efforts primarily focused on predicting Torsade de Pointes (TdP) risk (Ando et al., 2017; Blinova et al., 2018; Gintant et al., 2017; Gintant et al., 2020; Gintant and Traebert, 2020; Kanda et al., 2018; Millard et al., 2018; Pfeiffer-Kaushik et al., 2019; Ribeiro et al., 2019).

In the present study our aim was to expand beyond solely predicting TdP risk and use features of the high-resolution AP's generated in our model to determine its ability to predict clinical ECG endpoints including QTc and QRS. The high throughput format of our system allows for the generation of highly defined and reproducible concentration response data for multiple AP endpoints, providing the ability to measure subtle changes in these parameters over a broad concentration range. Importantly, the model can measure compound effects over a more extended time course in serum free conditions enabling the measurement of the effects of compounds with slow onset kinetics or those that affect surface ion channel expression without the issue of changes in free drug levels due to protein binding. We present data showing the ability of our model to provide a robust translation to several key clinical endpoints including QT and QRS intervals of the ECG, as well as TdP risk, highlighting its clear utility in early preclinical cardiac safety assessment of novel drug candidates.

2. Methods

2.1. Culture of hIPSC-CM's

Cryopreserved iCell^2 hIPSC-CM's (Cellular Dynamics International, Madison, WI, USA) were thawed and cultured in black walled optically clear plastic bottomed 96 well plates (Corning, Corning, NY, USA). Prior to seeding, wells were coated with 10 μg/mL bovine fibronectin (Sigma-Aldrich, St. Louis, MO, USA) for 1 h at 37 °C. Following media removal, cells were plated (50,000 cells per well: 100 μL per well) in iCell^2 plating media (Cellular Dynamics International, Madison, WI, USA). Cells were cultured at 37 °C in a humidified environment (5% CO_2/95% air). After 24 h, 100 μL of iCell^2 maintenance media (Cellular Dynamics International, Madison, WI, USA) was added to each well. Following an additional 24 h incubation the media was exchanged for maintenance media (200 μL per well). The maintenance media was subsequently exchanged every 2–3 days. Cells were cultured for a total of 8 days by which time they had formed an electrically coupled monolayer with synchronous beating.

2.2. Gene expression analysis

Human Cardiomyocyte samples were obtained from Anabios Corporation (San Diego, CA, USA). All human hearts used for this study were non-transplantable and ethically obtained by legal consent (first person or next of-kin) from organ donors in the United States. All recovery protocols were preapproved by the Institutional Review Boards (IRB) at each transplant center and the procurement processes are fully traceable and periodically reviewed by US Federal authorities. Upon arrival in the laboratory, hearts were re-perfused with an ice cold proprietary cardioplegic solution as previously described (Page et al., 2016). Adult human primary ventricular myocytes were isolated enzymatically from the ventricles. Digestion of the cardiac tissue was conducted at 37 °C for 25 min utilizing a proprietary solution which included a cocktail of proteolytic enzymes (Nguyen et al., 2017). Isolated cells were provided for this study as pellets snap-frozen in liquid nitrogen after isolation.

Total RNA was isolated from human primary ventricular myocytes and harvested iCell^2 hIPSCs using a Qiagen RNeasy micro kit (Qiagen, Germantown, MD, USA) in accordance with the manufacturer's protocol. Extracted RNA was quantified using a NanoDrop ND-1000 spectrophotometer (Thermo Fisher Scientific, Wilmington, DE, USA). The quality and quantity of the extracted RNA was assessed using an Agilent 4200 TapeStation system (Agilent Technologies, Santa Clara, CA, USA). First strand, then second strand cDNA was synthesized, amplified, fragmented, labeled, and hybridized using the Clariom D assay kit according to the manufacturer's protocol (Affymetrix, Santa Clara, CA, USA). The samples were prepared for hybridization and transferred to the GeneChip cartridge arrays. Arrays were incubated for 16 h in an Affymetrix GeneChip 645 hybridization oven at 45 °C with rotation at 60 rpm. The arrays were washed and stained using the Affymetrix GeneChip Fluidics Station 450. Finally, the arrays were scanned using an Affymetrix GeneChip Scanner 3000. Data was primarily analyzed using the Affymetrix Transcriptome Analysis Console software.

2.3. Measurement of cellular action potentials in hIPSC cardiomyocytes

High throughput measurements of hIPSC-CM's AP's were acquired optically using a fluorescent voltage sensitive dye methodology and the Photoswitch Bolt fast kinetic plate reader (Photoswitch Biosciences, Cleveland, OH, USA). This technology allows for simultaneous measurement of fluorescence changes across a 96 well assay plate at a capture rate of 10 kHz, thus allowing for a high-resolution capture of changes in the membrane potential.

The voltage sensitive dye used in this study, PhoS-VSD (Photoswitch Biosciences, Cleveland, OH, USA), has previously been described in the literature (Huang et al., 2015) and has excitation/emission peaks of 658 nM and 683 nM, respectively. The dye was dissolved at a concentration of 500 nM in serum-free FluoroBrite DMEM (Thermo Fisher, Waltham, MA, USA) containing HEPES (20 mM). Following media aspiration, the dye solution was added to each well (100 μL per well) and the plate was incubated for 15 min at 37 °C. The dye solution was subsequently removed and replaced with 180 μL of recording media (FluoroBrite DMEM/HEPES (20 mM)). The plate was returned to the cell culture incubator for 30 min before being placed in the Photoswitch Bolt instrument for an additional 30 min to allow for temperature equilibration. The instrument temperature was set at 28 °C. Measurement of the temperature across randomly selected wells (N = 10) demonstrated a mean assay plate temperature of 28 °C with a standard deviation of 0.1 °C after this 30 min incubation period.

Test compounds were dissolved and initially diluted in dimethyl sulfoxide (DMSO). Subsequent dilutions were then prepared in recording buffer, providing for 10x test solutions. Upon compound addition (20 μL) the final DMSO concentration in the assay was 0.1% (v/v). Each compound was tested across a range of 10 concentrations and concentration response curves were constructed.

During the assay, cells were excited at 660 nm and the change in fluorescence over time was measured at 680 nm. A 40 s baseline reading was obtained prior to the addition of test compounds. After addition of test compounds, the cells were equilibrated in the instrument for a further 30 min before a second 40 s read was performed. Assay plates were then returned to the incubator before being removed and returned to the Photoswitch Bolt 30 min prior to the final 24 h read. Fluorescent signals were analyzed using the proprietary analysis software from Photoswitch (version 1.1.7.27239), enabling the measurement of action potential duration (APD), beat rate and rise-time for each well.

2.4. hERG fluorescent polarization binding assay

Human embryonic kidney (HEK) cells stably transfected with a doxycycline inducible plasmid expressing the hERG channel (Accession Number: NM_000238) were cultured in suspension in Ex-cell 293 Serum-Free Medium (Sigma Aldrich, St Louis, MO, USA) containing fetal bovine serum (5% v/v), L-Glutamine (6 mM), Blasticidin (5 μg/mL) and Zeocin (600 μg/mL) at 37 °C in a humidified environment (5% CO_2/95% air). hERG expression was induced by the addition of doxycycline (1 μg/mL) 48 h prior to harvesting by centrifugation. Cell pellets were resuspended in ice cold homogenization buffer (1 mM EDTA, 1 mM EGTA, 1 mM $NaHCO_3$, and cOmplete™ protease Inhibitor cocktail). Cells were homogenized using a dounce homogenizer (20 strokes), and centrifuged (1,000×*g*) for 10 min at 4 °C. The supernatant was transferred to a new tube and was centrifuged a second time (25,000×*g*) for 20 min at 4 °C. The supernatant was discarded, and the pellet was resuspended in buffer (50 mM HEPES, 10 mM $MgCl_2$, bovine serum albumin (0.2% w/v) and cOmplete™ protease inhibitor cocktail). The samples were adjusted to 5 mg/mL and frozen.

For the assay, membrane aliquots were thawed on ice and diluted to 200 μg/mL in assay buffer (25 mM HEPES, 15 mM KCl, 1 mM $MgCl_2$, and 0.05% (v/v) Pluronic F127). A Cy3B tagged N-desmethyl dofetilide ligand was prepared in the same assay buffer solution (5 nM). Compound or vehicle (DMSO) was spotted into each well of a black 384-well low-volume plate. Membrane homogenate (15 μL) and Cy3B tagged ligand (10 μL) were then added to each well and the plate was incubated at room temperature for 16 h. Fluorescence polarization measurements were made using an Envision plate reader (PerkinElmer, Waltham, MA, USA) and mP values were used for analysis. Binding K_i values were determined using the Cheng-Prusoff equation ($K_i = IC_{50}/(1+L/K_d)$), where L was the labeled ligand concentration in the assay (2 nM), and the K_d value (1.35 nM) the affinity constant for the labeled ligand (Cheng and Prusoff, 1973).

2.5. Ion channel profiling

Chinese hamster ovary (CHO) cells stably expressing human $Ca_v1.2$/β2/α2δ1 calcium channel (Catalogue No. CT6004; Charles River Cleveland, OH, USA) were cultured in Ham's F12 medium supplemented with fetal bovine serum (FBS; 10% (v/v)), G418 (0.25 mg/mL), hygromycin (0.25 mg/mL), zeocin (0.4 mg/mL), and blasticidin (0.01 mg/mL). On the day prior to cell harvest, tetracycline (1 μg/mL) was added to the media to induce channel expression and the calcium channel antagonist verapamil (15 μg/mL) was added to minimize calcium-induced cytotoxicity. CHO cells stably expressing the human $Na_v1.5$ (sodium channel (Catalogue No. CT6007; Charles River Cleveland, OH, USA) were cultured in Ham's F12 media supplemented with 10% FBS (10% (v/v) and G418 (0.25 mg/mL).

All cell lines were cultured at 37 °C in a humidified environment (5% CO_2/95% air). On the day of the experiment, cells were harvested at 70–80% confluency by rinsing with Hank's Balanced Salt Solution and incubating for 2 min in Accutase (Innovative Cell Technologies, San Diego, CA, USA). Cells were resuspended (2 million cells per mL) in CHO-S-SFM II serum-free medium supplemented with 20 mM HEPES and were allowed to recover for 45 min with constant stirring prior to electrophysiological measurements. All tissue culture media and reagents were obtained from Thermo Fisher (Waltham, MA, USA), unless otherwise stated.

Ionic currents were evaluated in the whole-cell configuration using the Qube384 automated planar patch clamp platform (Sophion Bioscience A/S, Ballerup, Denmark). QChip 384X plates, containing 10 patch clamp holes per well, were used to maximize success rate, which was routinely >95%.

For $Ca_v1.2$ experiments, the external solution was composed of (in mM): 137.9 NaCl, 5.3 KCl, 0.49 $MgCl_2$, 10 $CaCl_2$, 10 HEPES, 0.34 Na_2HPO_4, 4.16 $NaHCO_3$, 0.41 $MgSO_4$, 5.5 glucose, pH 7.4, 312 mOsm. kg^{-1}. The internal solution contained (in mM): 27 CsF, 112 CsCl, 2 $MgCl_2$, 10 EGTA, 10 HEPES, 2 Na_2ATP, pH 7.2, 307 mOsm/kg. For $Na_v1.5$ experiments, the external solution was composed of (in mM): 137.9 NaCl, 5.3 KCl, 0.49 $MgCl_2$, 1.8 $CaCl_2$, 10 HEPES, 0.34 Na_2HPO_4, 4.16 $NaHCO_3$, 0.41 $MgSO_4$, 5.5 glucose, pH 7.4, and osmolarity of 303 mOsm.kg^{-1}. The internal solution contained (in mM): 92 CsF, 55 CsCl, 2 $MgCl_2$, 5 EGTA, 5 HEPES, 1 MgATP, pH 7.2, 298 mOsm.kg^{-1}. The osmolarity of the buffer was adjusted by the addition of sucrose as required.

The $Ca_v1.2$ current was elicited by a voltage step to 0 mV for 150 ms from a holding potential of −40 mV. Voltage steps were repeated at 0.05 Hz, and $Ca_v1.2$ amplitude was measured as the peak current at 0 mV. For the $Na_v1.5$ current, from an initial holding potential of −80 mV, a 200 ms prepulse to −120 mV was used to homogenize channel inactivation, followed by a 40 ms step to a test potential of −15 mV. Membrane potential was further depolarized to +40 mV for 200 ms to completely inactivate the peak $Na_v1.5$ current, followed by a ramp from +40 mV to −80 mV (−1.2 mV/ms). This voltage pattern was repeated at 0.2 Hz, with the $Na_v1.5$ peak current defined as the maximum current during the step to −15 mV. All studies were conducted at 23 °C.

Compounds were initially dissolved and diluted in DMSO, with a final dilution by the addition of external solution to generate final working concentrations. The final DMSO concentration in all experiments was 0.33% (v/v). Three vehicle periods each lasting 5 min were applied to establish a stable baseline, each well subsequently received a single concentration of compound. This application was repeated three times for each well, via a flowthrough addition where the solution was replaced with each addition. Each exposure lasted 10 min.

Patch clamp data were analyzed using Assay Software (Version 6.4.72; Sophion Bioscience A/S, Ballerup, Denmark). Current amplitudes were determined by averaging the last 4 currents under each test condition. The percent inhibition of each compound was determined by taking the ratio of current amplitude measured in the presence of various concentrations of the test compound ($I_{Compound}$) versus the vehicle control current ($I_{Vehicle}$):

$$\% \text{ Inhibition} = [1-(I_{Compound}/I_{Vehicle})] \text{ x } 100\%$$

A dose-response curve was generated IC_{50} value defined for each compound by fitting the data to a four-parameter logistical equation using the Sophion Analyzer software. The minimum response and slope were free fitted and maximum response was fixed to 100%.

2.6. Materials

All compounds were obtained from Sigma-Aldrich (St. Louis, MO, USA) with the exceptions of Mesoridazine, (ApexBio, Houston, TX, USA), Ribociclib (Tocris Bioscience, Minneapolis, MN, USA) and Vandetanib (Cayman Chemical Company, Ann Arbor, MI, USA).

2.7. Clinical data

Clinical concentration-QTc relationships were gathered from reference sources (Supplemental Table 2). Many of the studies highlighted had explicit concentration-QTc slopes or pharmacokinetic/pharmacodynamic (PK/PD) models described. These formulae were used to calculate QTc changes for a range of free plasma exposure concentrations that had been explored in the original reports (interpolation, rather than extrapolation). In some cases, concentration-QTc data were presented in a figure format within the paper or report, with or without a linear regression line for concentration-QTc. If a line was available this was digitized to extract slope data. When only concentration-QTc pairs were plotted these data were also digitized and a linear regression was used to calculate the slope of the concentration-QTc relationship. This slope was used to calculate QTc values for a similar concentration range to that explored in the published study. Finally, some data were only

available in the publications as limited discrete concentration and QTc datapoints where no slope could be practically estimated. These data were used as is. The concentrations were changed to molar units using molecular weight information from DrugBank (DrugBank.com) and the unbound concentration was calculated using publicly available plasma protein binding data (DrugBank, US product labels, FDA approval documents, or rarely separate publications). For a summary of the calculated free plasma exposures producing a 10 ms change in QTc, and the associated references, see Supplemental Table 2.

For a full description of the effective free therapeutic plasma concentration (EFTPC) for each compound, defined as the concentration of unbound compound in the plasma at a therapeutic dose, and associated references see Supplemental Table 3.

2.8. Curve fitting and modeling

For hIPSC-CM studies where concentration response curves were generated, responses in compound treated wells were normalized to two vehicle control wells located on the same row of the plate. Multiple endpoints including APDs, beat rate, and rise-time, were assessed using the Bolt software for each well. This measurement was repeated at 30 min and 24 h.

Concentration response curve analysis was performed as follows. The readout of a measurement was normalized to vehicle control wells of the curve via:

$$\text{Response} = \text{Readout/Mean (Vehicle)} \quad (1)$$

For each readout the data were further normalized by subtracting the median response value of the lowest two concentrations of all compounds. Response values from treatment groups annotated as having arrhythmia class 4–5 (see Supplemental Data 2 for details on arrhythmia classification) were removed prior to curve fitting. Models were fit using methods described in (Filer et al., 2017) with modifications. The Hill and gain-loss objective functions, optimized using maximum likelihood and a student's *t*-distributed error model, were fit in R 3.6.2 (R-Project, 2019) using the nloptr package to access NLopt 2.4.2 (Johnson, 2017) with optimization performed using the BOBYQA algorithm (Powell, 2009). The best model was selected based on the lowest AIC (Akaike, 1998).

Determining the free plasma drug exposure required to produce a 10 ms change in the clinical QTc was performed using the same methodology as above, with the exception that the data were not normalized.

TdP risk categories were defined primarily using the definitions provided by CredibleMeds.org and by CiPAProject.org. For a full description of the TdP risk categorization used in this study, and associated references, see Supplemental Table 4. Drugs categorized as a 'Known Risk' (defined at category 1 in Supplemental Table 4) were considered TdP positive while all others were considered TdP negative.

All machine learning models were generated using Caret 6.0–86 (Kuhn, 2020) and R 3.6.2 (R-Project, 2019). To determine the predictive performance of the models, 20 times repeated 5-fold cross validation was performed on each model. Features used in the models included curve fit parameters (Hill top, margin to the threshold concentration) and curve response values at multiples of the EFTPC for all the hIPSC-CM endpoints. Ion channel inhibition data (binding for hERG and patch clamp for $Ca_v1.2$ and $Na_v1.5$) was also incorporated into the modeling. This included direct ion channel inhibition percentages, as well as metrics calculated from waveforms generated by an in silico cardiomyocyte model (O'Hara et al., 2011) using an epicardial cell type at 60 beats per minute, and the exposure margin necessary to observe a 10 ms increase in the cardiomyocyte model APD_{90}. Features were explored individually and in combination using a variety of machine learning algorithms. These include logistic regression (stats package in base R), elastic net from glmnet 4.1 (Friedman et al., 2010), randomForest 4.6–14 (Liaw and Wiener, 2002), and recursive partitioning and regression trees from rpart 4.1–15 (Therneau and Atkinson, 2019).

2.9. Data and statistical analysis

Gene expression data were analyzed by means of an F-test to determine significant differences in gene expression across the whole data set using Transcriptome Analysis Console Software v4.0.1.36 (Thermo Fisher Scientific, Waltham, MA, USA). For comparisons of the expression of a specific target gene between iCell^2 and human ventricular cells a Welch's *t*-test was performed (Welch, 1947). Pearson correlation analysis of all non-censored data was performed using GraphPad Prism v9.00 software (RRID:SCR_002798, http://www.graphpad.com). A correlation comparison of non-censored or non-censored/censored data was performed using a Spearman rank analysis (Spearman, 1987). In all cases a P value of <0.05 was considered significant. n indicates the number of individual experiments or tissue samples.

To understand the ability of the hIPSC-CM model APD_{90} threshold values in predicting the clinical exposures producing a 10 ms QTc change or the IC_{50} concentration in the calcium patch clamp assay linear regression modeling was performed using a 4-fold cross validation with 10 repetitions. Performance metrics including the r^2 value and the root mean square error (RMSE) were reported. Similarly, a 5-fold cross validation was performed using hIPSC-CM rise-time values and the ratio of the clinical exposure associated with QRS prolongation/EFTPC to determine the predictivity of the assay with respect to defining clinical QRS risk.

Receiver-operator curve analyses that were not associated with the modeling efforts were performed using a webtool previously described by Goksuluk et al. (Goksuluk et al., 2016).

3. Results

3.1. GeneChip expression analysis

Gene expression was compared between iCell^2 hIPSC-CM's and purified human primary ventricular cardiomyocytes obtained from donor tissue (Supplementary Table 1). From a total of 48,243 transcripts, 37,494 (77.7%) did not significantly differ in expression between the two cell types, 6,785 transcripts (14.1%) were significantly upregulated, and 3,964 transcripts (8.2%) were significant downregulated in iCell^2 hIPSC-CM's compared with human primary cardiomyocytes (Fig. 1a). Gene expression data for all transcripts examined are available in Supplemental Data 2.

Several ion channels involved in the generation of the cardiomyocyte AP, including KCNH2 hERG (KCNH2) and $Ca_v1.2$ calcium channel (CACNA1C), showed similar expression levels (Fig. 1b). Differences in expression were observed for Kir2.1 (KCNJ2; responsible for I_{K1} current) and Kv4.3 (KCND3; responsible for I_{to} current), where expression of both was lower in the iCell^2 cardiomyocytes (12.4 and 8.7-fold, respectively). $Na_v1.5$ sodium channel (SCN5A) expression was significantly higher in the iCell^2 hIPSC-CM's; however, the absolute difference was small in magnitude (1.5-fold increase).

3.2. Measurement of hIPSC-CM action potential parameters

hIPSC-CM AP's were examined in voltage-sensitive dye-loaded cells. At an acquisition rate of 10 kHz, signals were captured at a resolution equivalent to those obtained by traditional patch clamp techniques, making it possible to accurately measure a wide variety of endpoints (Fig. 2a, b and c). The hERG channel blocker dofetilide produced a prolongation in the repolarization (Fig. 2a, d and 2g) following a 30 min or 24 h incubation. At 24 h higher concentrations of dofetilide (>10 nM) led to significant tachyarrhythmias (Fig. 2 g). The calcium channel blocker nifedipine shortened the APD at both time points (Fig. 2b, e and 2h), whereas the hERG trafficking blocker pentamidine had no effect on APD acutely, but did delay the repolarization after a 24 h incubation, in

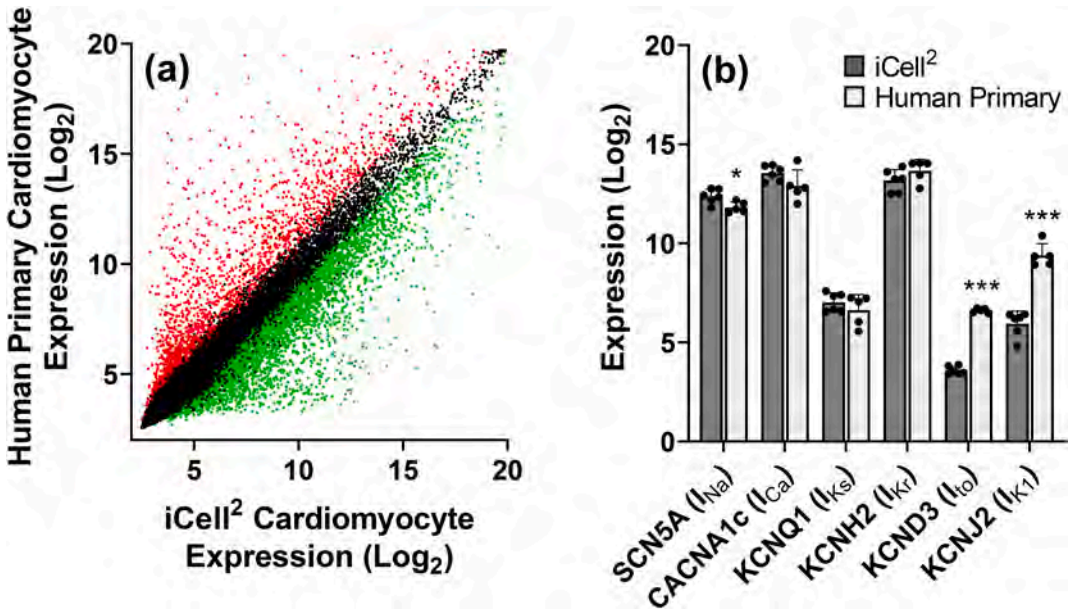

Fig. 1. GeneChip expression analysis of iCell^2 hIPSC cardiomyocytes and purified human primary ventricular cardiomyocytes. (a) Correlation of iCELL^2 hIPSC cardiomyocytes (n = 6) and purified human primary ventricular cardiomyocytes (n = 5) transcript expression. A total of 48,234 transcripts were compared (significantly higher expression in iCell^2 cells highlighted in green ($P < 0.05$; F-Test); significantly lower expression in iCell^2 cell in red ($P < 0.05$, F-Test); no difference in expression in black). (b) Comparison of expression of key ion channels involved in cardiac action potential generation between iCell^2 cardiomyocytes (n = 6) and human primary cardiomyocytes (n = 5). Values are expressed as mean ± SD. Statistically differences in channel transcript expression between iCell^2 and human primary cardiomyocytes are shown (*$P < 0.05$; ***$P < 0.001$; Welch's *t*-test).

line with the membrane turnover of the hERG channel ($T_{1/2}$ of ~11 h) (Ficker et al., 2003).

The QT interval of the ECG and APD are both rate dependent. QT interval can be corrected for beat rate using several correction formulae, such as Bazett's (Bazett, 1920) or Fridericia (1920). A more recent correction proposed by Yamamoto et al. (2016), may be more suited for use with hIPSC-CM's. Fig. 2j highlights the distribution of APD_{90} measurements from vehicle treated cells compared to their corresponding RR interval (beat to beat interval). APD_{90} refers to the time required for the AP to repolarize by 90%. As expected, as the beat rate slows, and the RR interval increases, the APD_{90} values increase. Employing Bazett's, Fridericia's or Yamamoto's formulae resulted in a correction in APD_{90} (Fig. 2k and l). The vehicle treated correlation generated a slope of 0.130 ± 0.005, which was reduced to −0.010 ± 0.003 using Bazett's, 0.022 ± 0.004 with Fridericia's and −0.005 ± 0.003 with Yamamoto's correction formulae. With the resultant slope being the closest to zero, the Yamamoto correction was deemed the most appropriate correction formula for the present study.

In addition, to avoid issues associated with changes in free drug levels due to protein binding, assays were run in serum free conditions. The impact of serum free conditions on baseline vehicle parameters was examined both acutely (30 min) and chronically (24 h). ADP_{90} values were significantly greater in serum free versus serum containing conditions at both time points, as was the rise-time and $cAPD_{90}$, with beat rate found to be lower in serum free conditions (Supplemental Fig. 2). Overall, the removal of serum did not significantly affect the morphology or visual health of the cells over the time period examined.

3.3. Correlation of hIPSC-CM action potential duration to clinical QTc interval

A key aim in the development of an in vitro hIPSC-CM model is the ability to predict compound-mediated changes in the clinical QTc interval. With the expression of multiple ion channels involved in the generation of the cardiac AP present in hIPSC-CM's, they have the potential to predict not only QTc changes associated with selective hERG channel blockers, but also integrated responses for compounds that possess multi-ion channel pharmacology. With that goal, 29 compounds were selected for which clinical QTc data were available (Table 1). Concentration-response curves were generated for each compound in the hIPSC-CM model and the concentration of each compound that produced a positive threshold increase in APD_{90} was determined (defined as three times the standard deviation of baseline values, an increase of 10.3% and 7.94% for the 30 min and 24 h time points, respectively). All curve fitting was performed using an automated curve fitting algorithm to avoid bias, as described in section 2.8. A single curve fit was performed per compound using averaged APD_{90} data for each concentration tested (n ≥ 3 independent experiments per compound). A similar method was used to define the compound exposure required to produce a 10 ms increase in the clinical QTc interval (Table 1).

Independent Pearson correlation analyses were performed comparing various endpoints that included APD_{90}, Yamamoto-corrected APD_{90} ($cAPD_{90}$), clinical QTc data or hERG binding data (Fig. 3), to determine which endpoint correlated best with the clinical QTc response. Since not all compounds reached the defined threshold value (i.e. data where the concentration values have a > prefix, defined here as censored values), we also performed Spearman rank correlation analyses to ensure that both non-censored and censored data were included in the analysis (Table 2). An excellent correlation was observed between the concentration of compound producing a threshold increase in hIPSC-CM APD_{90} and the concentration producing a 10 ms increase in the clinical QTc interval (Fig. 3a). Statistical analysis using either a Pearson or Spearman rank correlation highlighted that the 24 h timepoint in the hIPSC-CM assay correlated more closely with the clinical QTc than the corresponding 30 min timepoint (Table 2). Correlations were similar when comparing $cAPD_{90}$ values, or when hERG binding pK_i values were substituted for the APD_{90} values (Fig. 3b). In addition, there was also a robust correlation between APD_{90} and hERG pK_i values (Fig. 3c) whether looking more specifically at the smaller subset of compounds that had associated clinical QTc data available (24 h timepoint: $r^2 = 0.757$; n = 23) or the larger compound set used in this study ($r^2 = 0.718$; n = 42).

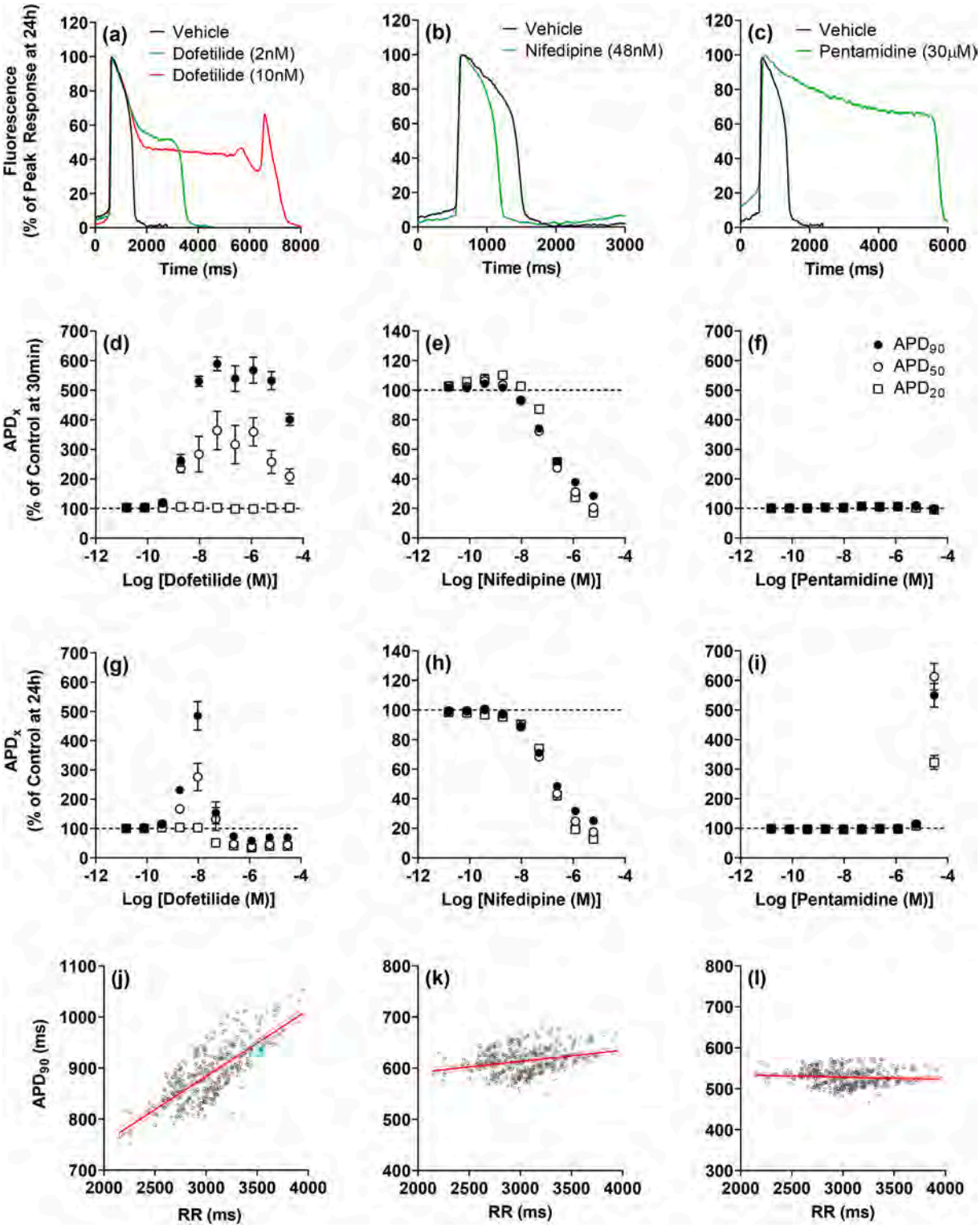

Fig. 2. Effect of standard compounds on the iCell^2 hIPSC-CM action potential. (a–c) Example recording of action potentials following 24 h incubation with (a) the hERG blocker dofetilide, (b) the calcium channel blocker nifedipine, and an inhibitor of hERG trafficking, pentamidine. Concentration response curves for the effects of standard compounds on action potential durations for 20% (APD_{20}), 50% (APD_{50}), and 90% (APD_{90}) recovery following an acute 30 min (d–f) or chronic 24 h (g–i) treatment. Data represent the mean ± the standard error of the mean from a series of independent experiment (dofetilide (n = 6), nifedipine (n = 3) and pentamidine (n = 6)). Effect of action potential corrected for heart rate on APD_{90} in vehicle treated iCell^2 hIPSC-CM's. (j) Uncorrected values (Slope = 0.130 ± 0.005), or values corrected using the (k) Fridericia (Slope = 0.022 ± 0.004), or (l) Yamamoto (Slope = −0.005 ± 0.003) correction formulae. Data represent a total of 384 individual data points (n = 24 independent experiments, 16 data points per experiment). The optimal linear regression analysis fit is shown by the solid red line and the 95% confidence intervals of the fit represented by the dashed red lines.

Table 1
Effect of compounds on iPSC cardiomyocyte APD_{90}, hERG channel binding and clinical QTc interval.

	Threshold Drug Concentration for hiPSC-CM Endpoint Log [Concentration (M)]				hERG Binding	Clinical QTc
Compound	APD_{90} (30 min)	APD_{90} (24 h)	$cAPD_{90}$ (30 min)	$cAPD_{90}$ (24 h)	Log K_i (M) ± SD (*n*)	Free Exposure Producing 10 ms Change Log [Concentration (M)]
Azimilide	−6.57	−7.23	−6.59	−7.42	−6.46 ± 0.02 (3)	−7.93
Bepridil	−7.24	−6.84	−7.57	−6.90	−7.14 ± 0.04 (6)	−7.93
Cisapride	−8.14	−7.50	−8.39	−7.54	−7.73 ± 0.05 (6)	−8.38
Citalopram	−6.47	−6.64	−6.54	−6.78	−5.39 ± 0.04 (3)	−6.78
Dofetilide	−9.40	−9.65	−9.55	−9.70	−8.48 ± 0.08 (6)	−9.37
Droperidol	−7.95	−7.04	−8.14	−7.77	−6.86 ± 0.24 (6)	−7.40
E4031	−8.65	−9.01	−8.87	−9.12	−7.11 ± 0.04 (3)	−8.65
Halofantrine	−6.46	−7.22	−6.55	−7.10	−7.52 ± 0.12 (3)	−7.24
Ibutilide	−9.30	−8.89	−9.41	−9.07	−8.11 ± 0.18 (6)	−9.95
Lamotrigine	> −4.52	> −4.52	> −4.52	> −4.52	> −4.10 (3)	> −4.61
Levocetirizine	−4.65	−4.92	−4.64	−4.81	−4.40 ± 0.07 (3)	> −6.88
Levofloxacin	−4.70	−4.72	−4.70	−4.72	> −4.10 (3)	> −5.54
Mesoridazine	−6.40	−6.90	−6.47	−7.00	−5.32 ± 0.04 (3)	−6.63
Moxifloxacin	−4.54	−5.07	−4.53	−4.98	−4.38 ± 0.11 (3)	−5.70
Odansetron	−6.40	−6.42	−6.43	−6.47	−5.64 ± 0.10 (6)	−6.59
Paliperidone	−6.90	−6.81	−6.95	−6.99	−5.84 ± 0.15 (6)	> −7.52
Procainamide	−5.37	−4.83	−5.22	−4.90	−3.85 ± 0.19 (4)	−4.83
Quinidine	−6.78	−6.56	−6.86	−6.67	−5.72 ± 0.19 (6)	−6.73
Quinine	−6.78	−6.47	−6.74	−6.48	−4.88 ± 0.14 (3)	−5.59
Ranolazine	−5.86	−5.59	−6.24	−5.59	−4.61 ± 0.02 (3)	−5.85
Ribociclib	−5.82	−6.07	−5.60	−5.99	−4.73 ± 0.04 (3)	−7.38
Risperidone	−7.35	−7.15	−7.36	−7.25	−6.27 ± 0.09 (6)	> −7.44
Sotalol	−5.57	−4.77	−5.46	−4.38	−4.72 ± 0.15 (6)	−6.12
Terfenadine	−7.86	−7.03	−8.46	−7.24	−7.78 ± 0.14 (6)	−8.18
Terodiline	−6.93	−7.14	−7.02	−7.14	−6.04 ± 0.08 (3)	−7.64
Thioridizine	−6.72	−7.11	−6.74	−7.22	−6.64 ± 0.08 (3)	−7.43
Tolterodine	−8.41	−8.53	−8.47	−8.52	−7.60 ± 0.18 (3)	−8.67
Vandetanib	−6.73	−7.04	−6.52	−7.05	−6.28 ± 0.03 (3)	−7.66
Verapamil	>−4.52	>−4.52	>−4.52	>−4.52	−5.94 ± 0.32 (6)	> −7.43

References for clinical QTc data can be found in supplemental data (Table S2).

To determine the ability of the hIPSC-CM model or the hERG binding to predict a 10 ms change in the clinical QTc interval, a 4-fold cross validation analysis was performed using APD_{90} threshold (increase) values or hERG pK_i values (i.e. 4/5 of the data set for each parameter were used to build the linear regression model and 1/5 was used as the test set, this cross validation was repeated 10 times with the data being randomly assigned to each set with each repeat). For the hIPSC-CM APD_{90} values the r^2 value was 0.84 (i.e. the data explain 84% of the variability in the clinical QTc data) with a root mean square error (RMSE) of $Log_{10} = 0.64$, which translates to an error of 4.4-fold. In contrast for hERG pK_i values the r^2 value was slightly higher at 0.86 with a RMSE of $Log_{10} = 0.60$, which translates to an error of 4.0-fold. Using the Pearson correlation of non-censored data allowed for the generation of correlation equations for each assay (Table 2), that can be used to define an estimation of the clinical QTc effects using either hIPSC-CM or hERG pK_i endpoints.

3.4. Prediction of TdP risk using hIPSC-CM endpoints

Several features from the hIPSC-CM assay endpoints were evaluated for their ability to predict clinical TdP. These include curve fit parameters (Hill top) and values calculated from the Hill model in the context of the EFTPC. The latter includes the margin between the plasma concentration and the concentration at which the Hill model crosses the baseline threshold for that endpoint. In addition, the amplitude of the response values at 1, 3, 10, 30, and 100-fold the EFTPC were calculated from the Hill model. These are labeled as MRYYx with the 'YY' indicating the multiple (i.e. MR30x for maximal response at 30x EFTPC).

Models constructed using individual response values at multiples of EFTPC were predictive, with area under receiver-operator curve (AUROC) values in the range of 0.84–0.92 for the most predictive models trained using categorization trees and logistic regression. These models consistently found higher AUROC values from $APD_{50/80/90}$ endpoints, with a slight benefit to the corrected APD values. The maximum APD_{90} response at 30x the effective therapeutic plasma concentration (MR30x) values were among the most predictive.

Combinations of features were explored to see if model performance could be improved. An elastic net model trained on all maximal response values had a AUROC of 0.885; limiting to just the MR30x values had a similar performance (AUROC of 0.899). Further improvement was found using randomForest models on subsets of the more predictive features. Ultimately the optimal model, with both the highest AUROC (0.938) and Matthew's Correlation Coefficient (MCC) (0.736) (Matthews, 1975), was a randomForest model trained using the MR30x values from the 24 h $cAPD_{90}$ and $cAPD_{50}$ endpoints, as well as the Hill top values from the same curves (Table 3 and Fig. 3d). The ability of this model to correctly predict TdP risk for individual compounds is highlighted in Fig. 3e and in Supplemental Table 5. In addition, the impact of this model on determining the posttest probability of a positive TdP liability when used as a follow up assay to hERG and in vivo QTc profiling is highlighted in the decision tree in Table 4.

Results from the ion channel assays were also explored. Ion channel blocks were calculate as described in (Lancaster and Sobie, 2016) and were used in the O'Hara-Rudy cardiomyocyte model to generate membrane potential and calcium waveforms (O'Hara et al., 2011). These were run at a wide range of assumed drug concentrations to generate waveforms at multiples of the EFTPC, and the compound concentrations producing a 10 ms change in APD_{90} were calculated. Subsequent modeling analysis included ion channel block values directly, metrics calculated from the waveforms as described (Lancaster and Sobie, 2016), and the margin necessary to generate a 10 ms APD_{90} increase.

Ion channel features alone were not as predictive as models trained on the hIPSC-CM data. Incorporating ion channel features with the hIPSC-CM data did not generate models that were more predictive than the hIPSC-CM features alone (Table 3).

A detailed summary of the prediction of each compound in each

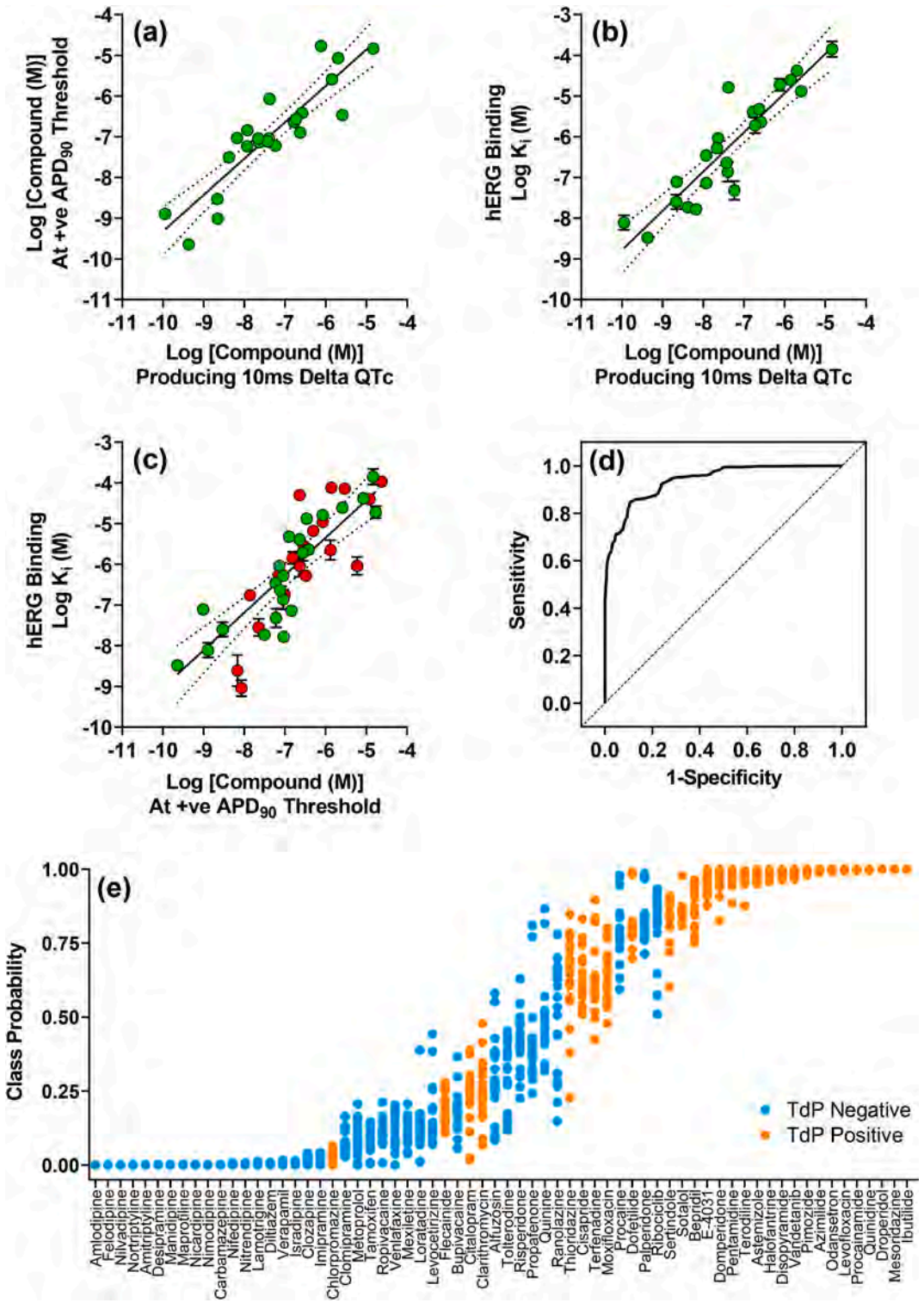

Fig. 3. Correlation analysis of compounds concentrations required to produce a positive threshold change (defined as three times the standard deviation of control values) in hIPSC-CM (a) APD_{90} with the compound concentration required to produce a positive 10 ms change in QTc in the clinic. (b) Correlation of hERG binding (Log K_i) with compound concentration required to produce a 10 ms change in QTc in the clinic. For (a) data represent values from 23 compounds (compound list available in Supplemental Data 1). (c) Correlation of hERG binding (Log K_i) with compound concentration required to produce a threshold increase in APD_{90}. Data highlighted by green symbols represent compounds shown in (a–b). Data highlighted in red show correlation including an additional 19 test compounds where clinical QTc data were not available (compound list available in Supplemental Data 1). Dotted lines represent the 95% CI of the linear fit. Data represent the mean. The standard deviation of the mean is shown for hERG binding data. (d) AUROC plot for the randomForest model trained using the maximum APD_{90} response at 30x the effective therapeutic plasma concentration (MR30x) values from the Yamamoto-corrected APD_{90} and APD_{50} endpoints from the 24 h time point, as well as the Hill top values from the same curves (n = 66 compounds, AUROC value = 0.938). (e) Class probabilities of TdP classification using the model highlighted in (d). The class probabilities from the 20x repeated 5-fold cross validation predictions are indicated for each compound. The y-axis indicates the numeric value of the class probability, with points greater than 0.5 predicted as TdP positive and those below this cutoff as TdP negative. Orange points below 0.5 and blue points above 0.5 are mispredictions.

Table 2
Summary statistics for correlation of hIPSC-CM APD_{90} values and hERG binding to clinical QTc.

Endpoint Comparison			Spearman Rank Correlation (ρ Value)		Pearson Correlation (r^2 Value)	
hIPSC-CM Assay Incubation Time	X-Axis	Y-Axis	Non-Censored Data	All Data	Non-Censored Data	Correlation Equation
30 min	QTc	APD_{90}	0.799 (23)	0.767 (29)	0.762 (23)	Y = 0.86X – 0.64
30 min	QTc	$cAPD_{90}$	0.841 (23)	0.795 (29)	0.737 (23)	Y = 0.92X – 0.35
30 min	APD_{90}	hERG Binding	0.785 (23)	0.807 (29)	0.786 (23)	Y = 0.95X + 0.39
30 min	$cAPD_{90}$	hERG Binding	0.823 (23)	0.838 (29)	0.799 (23)	Y = 0.89X + 0.04
24 h	QTc	APD_{90}	0.882 (23)	0.822 (29)	0.800 (23)	Y = 0.89X – 0.39
24 h	QTc	$cAPD_{90}$	0.893 (23)	0.818 (29)	0.776 (23)	Y = 0.93X – 0.17
24 h	APD_{90}	hERG Binding	0.842 (23)	0.860 (29)	0.757 (23)	Y = 0.92X + 0.18
24 h	$cAPD_{90}$	hERG Binding	0.847 (23)	0.861 (29)	0.755 (23)	Y = 0.87X – 0.13
–	QTc	hERG Binding (pK_i)	0.883 (23)	0.889 (29)	0.832 (23)	Y = 0.96X + 0.85

$P < 0.0001$ for all correlations shown. Number of compounds included in correlation shown in parenthesis. $cAPD_{90}$; Yamamoto corrected APD_{90} values. QTc, APD_{90}, $cAPD_{90}$, and hERG binding used in this analysis can be found in Table 1.

Table 3
Overview of Torsades de Pointes predictive modeling analysis.

Assay Format	Inputs	Features	Method	AUROC	MCC	TP	TN	FP	FN
Stem Cell	Multiple	modl_tp_24h_ycAPD50 modl_tp_24h_ycAPD90 MR30x_24h_ycAPD50 MR30x_24h_ycAPD90	randomForest	0.938	0.736	24.70	32.70	4.30	4.30
Stem Cell/Ion Channel	Multiple	modl_tp_24h_ycAPD50 modl_tp_24h_ycAPD90 MR30x_24h_ycAPD50 MR30x_24h_ycAPD90 gherg/gcav/gnavp	randomForest	0.930	0.734	24.80	32.55	4.45	4.20
Stem Cell	Single	MR10x_0.5h_ycAPD90	Logistic Regression	0.917	0.676	21.30	34.10	2.90	7.70
Ion Channel/O'Hara Model	Multiple	logconcM_10 ms_margin	Logistic Regression	0.845	0.627	23.90	29.85	7.15	5.10
Ion Channel	Multiple	gherg/gcav/gnavp	randomForest	0.819	0.496	20.35	29.30	7.70	8.65

All data represent 20 times 5-fold cross validation analyses. AUROC: area under receiver operator curve; MCC: Matthews correlation coefficient; TP: true positive; TN: true negative; FP: false positive; FN: false negative; MR10x or MR30x: maximum response within a 10x or 30x margin of the EFTPC; modl_tp: maximum asymptote of curve fit at any concentration; ycAPD50 or ycAPD90: Yamamoto-corrected action potential duration 50 or 90; 0.5h or 24h: 0.5 h or 24 h assay incubation time; gherg/gcav/gnavp calculated fractional block of hERG/Cav1.2/Nav1.5 (peak) at a 30x multiple of the EFTPC; logconcM_10 ms_margin: calculated concentration of compound required to produce a 10 ms increase in action potential duration using the output of O'Hara-Rudy modeling of ion channel data (O'Hara et al., 2011).

Table 4
Impact of hIPSC-CM Model on predicting the probability of TdP liability.

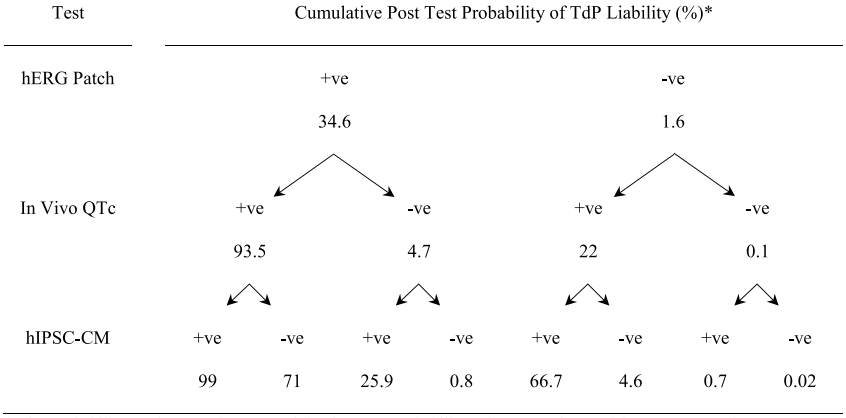

*Prior probability used = 10%. hERG patch/in vivo QTc probability values are referenced from Vargas et al. (2021).

model can be found in Supplemental Fig. 1.

3.5. Translation of hIPSC-CM's action potential rise-time to clinical QRS prolongation

Cardiac sodium channels, such as $Na_v1.5$, are essential for the rapid depolarization that initiates a ventricular AP, and their inhibition results delayed conduction and a prolongation of the QRS interval of the ECG. If large enough this has the potential lead to cardiac arrhythmias (Tan et al., 2003). Here we examined AP rise-time (i.e. time from the initiation of depolarization to the maximum depolarization), as a surrogate of conduction delay due to sodium channel inhibition, to determine if this endpoint was predictive of clinical QRS prolongation. From rise-time concentration response curves we compared the compound concentration required to produce a threshold increase in AP rise-time following curve fitting as described in section 2.8 (defined as three times the

Table 5
Effect of compounds on clinical QRS interval, hIPSC-CM action potential rise time and $Na_v1.5$ patch clamp.

Compound	Clinical Data		hIPSC-CM Data	$Na_v1.5$ Patch Clamp Data		
	Clinical QRS Prolongation Observed	Clinical Free Exposure (μM)	Rise Time Threshold Concentration At 24 h (μM) (Ratio vs. Clinical Exposure)	IC_{50} (μM) (Ratio vs Clinical Exposure)		
				Period 1	Period 2	Period 3
Amitriptyline	Yes	0.17	1.6 (9)	1.8 (11)	1.1 (6)	0.9 (5)
Astemizole	No	0.0036	0.1 (28)	3.3 (917)	2.0 (556)	1.5 (417)
Bepridil	No	0.03	3.2 (107)	7.5 (250)	3.3 (110)	2.3 (77)
Bupivacaine	Yes	0.21	8.3 (40)	4.8 (23)	3.8 (18)	3.1 (15)
Carbamazepine	Yes	62.72	119.0 (2)	602.6 (10)	446.7 (7)	398.1 (6)
Chlorpromazine	No	0.04	13.4* (335)	3.6 (90)	2.0 (50)	1.4 (35)
Cisapride	No	0.003	1.5 (500)	11.4 (3800)	6.2 (2067)	4.6 (1533)
Citalopram	Yes	1.20	7.9 (7)	46.9 (39)	39.6 (33)	35.7 (30)
Clomipramine	No	0.02	8.9* (445)	2.6 (130)	1.9 (95)	1.4 (70)
Clozapine	No	0.07	13.4* (191)	17.5 (250)	13.3 (190)	9.0 (129)
Desipramine	Yes	0.12	1.7 (14)	2.7 (23)	1.6 (13)	1.4 (12)
Disopyramide	Yes	1.82	21.9 (12)	396.0 (218)	288.3 (158)	189.4 (104)
Domperidone	No	0.02	1.1 (55)	10.0 (500)	3.7 (185)	3.3 (165)
Flecainide	Yes	0.12	1.4 (12)	16.9 (141)	12.0 (100)	10.6 (88)
Imipramine	Yes	0.04	2.3 (58)	2.6 (65)	1.1 (28)	1.1 (28)
Lamotrigine	Yes	26.01	6.9 (0.3)	433.2 (17)	332.3 (13)	240.9 (9)
Loratadine	No	0.0005	3.0 (6000)	44.7 (84900)	31.4 (62800)	20.8 (41600)
Maprotiline	Yes	0.06	1.8 (30)	2.3 (38)	1.5 (25)	1.2 (20)
Mesoridazine	Yes	2.07	1.6 (1)	12.9 (6)	9.1 (4)	8.0 (4)
Mexiletine	Yes	1.03	20.4 (20)	95.5 (93)	49.4 (48)	41.8 (41)
Moxifloxacin	No	2.84	>300.0 (>106)	>1000.0 (>352)	>1000.0 (>352)	>831.8 (>293)
Nicardipine	No	0.01	0.7* (70)	9.6 (960)	4.9 (490)	3.3 (330)
Nortriptyline	Yes	0.03	0.8 (27)	1.8 (60)	1.1 (37)	0.9 (30)
Pimozide	No	0.001	0.2 (200)	3.3 (3300)	1.4 (1400)	1.2 (1200)
Procainamide	Yes	26.01	329.0 (13)	1957.1 (75)	1512.6 (58)	1238.9 (48)
Propafenone	Yes	0.15	0.8 (5)	2.8 (19)	1.7 (11)	1.3 (9)
Quinidine	Yes	1.08	9.6 (9)	19.8 (18)	14.4 (13)	13.3 (12)
Quinine	Yes	0.81	13.1 (16)	53.2 (66)	45.7 (56)	34.2 (42)
Risperidone	Yes	0.31	7.5 (24)	76.6 (247)	54.1 (175)	45.0 (145)
Ropivacaine	Yes	2.51	22.9 (9)	22.6 (9)	17.1 (7)	13.0 (5)
Sertindole	No	0.002	0.3 (150)	6.8 (3400)	2.7 (1350)	1.7 (850)
Terfenadine	No	0.009	2.7* (300)	3.3 (367)	2.0 (222)	1.5 (167)
Thioridazine	Yes	0.82	1.1 (1)	3.8 (5)	2.1 (3)	1.5 (2)
Venlafaxine	Yes	22.71	108.4 (5)	245.5 (11)	177.4 (8)	160.1 (7)

standard deviation of the baseline data, a change of 1.72% from baseline) with compounds that had been clinically associated, or not associated, with QRS prolongation at a measured free plasma concentration. For several compounds profiled in this study an increase in AP rise-time was not detected, however an abrupt cessation of beating was observed as the compound concentration was increased. Since the Hill slope of the inhibition of sodium channel activity can be steep, it is likely that this rapid transition from beating to quiescence is sodium channel mediated. In such cases the concentration selected for analysis was the geometric mean concentration that fell between where the cells showed normal AP morphology and those that were quiescent.

For compounds to be included in this analysis the clinical exposure data presented in the literature had to be time-matched with the observed QRS measurement. As with previous studies in this area

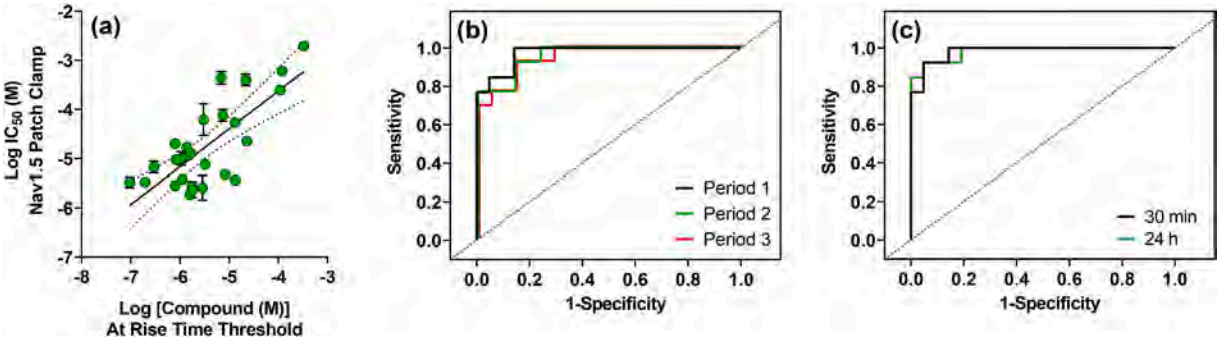

Fig. 4. Comparison of hIPSC-CM action potential rise-time, $Na_v1.5$ channel inhibition with clinical QRS prolongation. (a) Correlation of compounds concentrations required to produce a positive threshold change (defined as three times the standard deviation of control values) in hIPSC-CM action potential rise-time (24 h incubation time point) versus the IC_{50} value generated in a $Na_v1.5$ patch clamp assay (incubation period 1 only). (b) Receiver operator curve analysis of comparing $Na_v1.5$ patch clamp assay IC_{50} values (incubation period 1, 2 or 3) divided by the clinical free exposure versus the risk of an increase in QRS interval as defined by a published clinical observation (n = 34 compounds) (compound list available in Supplemental Data 1). (c) Receiver operator curve analysis of comparing ratio of rise-time threshold concentration in hIPSC-CM assay (30 min or 24 h incubation) divided by the clinical free exposure versus the risk of an increase in QRS interval as defined by a published clinical observation (n = 34 compounds). A full analysis is shown in Table 6. Data represent the mean. The standard deviation of the mean is shown for patch clamp data.

Table 6
Summary statistics for receiver-operator curve analysis of hIPSC-CM rise time, $Na_v1.5$ patch clamp and clinical QRS data.

Assay Format	Incubation	AUROC Value (95% CI)	Sensitivity Value (95% CI)	Specificity Value (95% CI)	Cut Point Value	n Value
hIPSC-CM	30 min	0.982 (0.949, 1.014)	0.922 (0.640, 0.998)	0.952 (0.762, 0.999)	33.0	34
hIPSC-CM	24 h	0.982 (0.948, 1.016)	0.922 (0.640, 0.998)	0.952 (0.762, 0.999)	56.4	34
$Na_v1.5$ Patch	Period 1	0.974 (0.934, 1.015)	1.000 (0.753, 1.000)	0.857 (0.637, 0.970)	95.0	34
$Na_v1.5$ Patch	Period 2	0.960 (0.904, 1.016)	0.923 (0.640, 0.998)	0.857 (0.637, 0.970)	93.1	34
$Na_v1.5$ Patch	Period 3	0.953 (0.890, 1.015)	0.923 (0.640, 0.998)	0.857 (0.637, 0.970)	70.1	34

95% CI; 95% confidence intervals. n value represents the number of compounds included in the analysis.

(Harmer et al., 2011), due to the lack of extensive clinical studies focusing on QRS interval measurement, we expanded our criteria to include single case reports and reports of compound overdose, however the requirement for time-matched exposure/QRS measurements was maintained.

A total of 35 compounds were selected, 21 associated with QRS prolongation and 14 not associated (Table 5). For QRS positive compounds, the ratio of the concentration required to produce a threshold increase in AP rise-time in the hIPSC-CM's over the lowest reported clinical exposure associated with QRS was calculated. For QRS negative compounds the ratio of the concentration producing an increase in threshold AP rise-time over the highest reported exposure was defined. For many compounds this equated to their EFTPC that would be observed during normal therapeutic use. These ratios were used in combination with a binary definition of QRS prolongation liability to perform a receiver-operator curve (ROC) analysis to determine if increases in hIPSC-CM AP rise-time were associated prolongation of the clinical QRS interval. In addition, for comparison a similar analysis was performed using $Na_v1.5$ patch clamp data, with the analysis being subdivided by the compound addition period. These equated to period 1 (one compound addition; 10 min total incubation), period 2 (two compound additions; 20 min total incubation) or period 3 (three compound additions; 30 min total incubation).

ROC analysis of the patch clamp data highlighted AUROC values of 0.974, 0.960 and 0.953 with respect to the data from the period 1, 2 and 3, respectively (Fig. 4 and Table 6). Moreover, analysis of period 1 patch clamp data showed the highest-level sensitivity/specificity with values of 1.00 and 0.86, respectively, when using an optimal cut-off value defined using the ROC01 analysis methodology (Goksuluk et al., 2016). hIPSC-CM AUROC values were slightly higher with an identical AUROC value of 0.982 observe for both the 30 min and 24 h time points (Table 6).

To determine the ability of the hIPSC-CM model to predict clinical QRS risk, a 5-fold cross validation analysis, repeated 10 times, was performed comparing AP rise-time threshold values with the ratio of the clinical exposure associated with QRS prolongation/EFTPC in an ROC analysis. This analysis resulted in a decrease in the AUROC values for the patch clamp assay (0.918, 0.909 and 0.903 for the period 1, 2 and 3, respectively), however the hIPSC-CM data AUROC values were maintained with value of 0.980 (sensitivity/specificity: 0.941/0.837) at the 30 min time point.

3.6. Translation of hIPSC-CM's action potential duration to calcium channel inhibition

Calcium channel inhibition leads to a reduction in APD in cardiomyocytes (Lee et al., 2016). In the present study we examined the correlation between the concentration of compound required to produce a threshold reduction (defined as three times the standard deviation of the control data, a change of 11% from baseline) in APD_{90} versus IC_{50} values for calcium current inhibition in a $Ca_v1.2$ patch clamp assay. All compounds from the broader compound test set that generated a threshold reduction in APD_{90} were included in the analysis. A correlation was observed between uncorrected APD_{90} threshold concentration values and calcium channel patch clamp IC_{50} values ($r^2 = 0.80$; n = 16) (Fig. 5a). In hIPSC-CM's calcium channel antagonists are known to produce an increase in beat rate, an effect that is the opposite from what is observed in primary ventricular cardiomyocytes (Zeng et al., 2019). This effect was also observed in the present study where we found a correlation between the concentration of compound required to produce a threshold increase in beat rate values (defined as three times the standard deviation of the vehicle control data) with the calcium channel patch clamp IC_{50} values ($r^2 = 0.67$; n = 14) (Fig. 5b). Correcting the APD_{90} values for the change in beat rate using the Yamamoto formula led to an improved correlation ($r^2 = 0.87$; n = 17) (Fig. 5c).

To determine the ability of the hIPSC-CM model to predict the

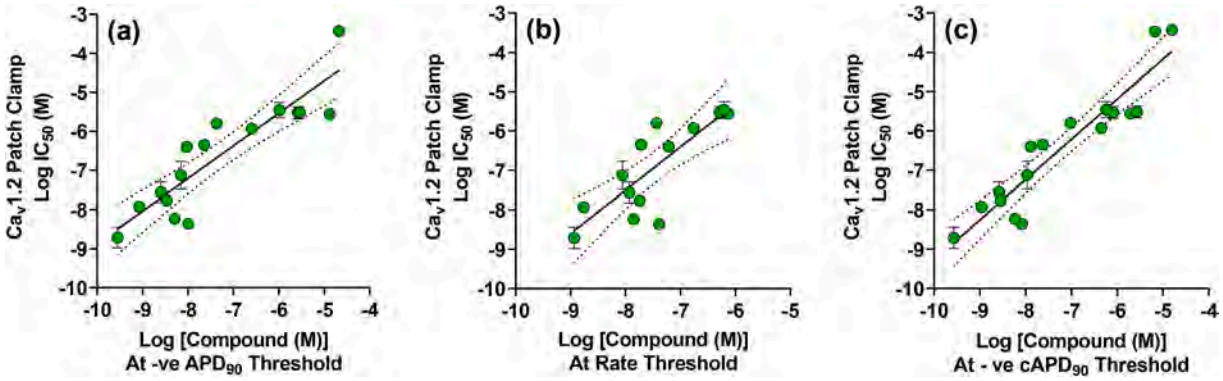

Fig. 5. Effect of calcium channel antagonists on APD_{90} in hIPSC-CM's. (a) Correlation of compounds concentrations required to produce a negative threshold change (defined as three times the standard deviation of control values) in hIPSC-CM APD_{90} versus the IC_{50} value generated in a $Ca_v1.2$ patch clamp assay (n = 16 compounds) (compound list available in Supplemental Data 1). (b) Correlation of compounds concentrations required to produce a positive threshold change (defined as three times the standard deviation of control values) in hIPSC-CM beat rate versus the IC_{50} value generated in a $Ca_v1.2$ patch clamp assay (n = 14 compounds) (compound list available in Supplemental Data 1). (c) Correlation of compounds concentrations required to produce a negative threshold change (defined as three times the standard deviation of control values) in hIPSC-CM $cAPD_{90}$ (i.e. corrected for increases in beat rate) versus the IC_{50} value generated in a $Ca_v1.2$ patch clamp assay (n = 17 compounds) (compound list available in Supplemental Data 1). Data represent the mean. The standard deviation of the mean is shown for patch clamp data.

calcium channel inhibition in the patch clamp assay, a 4-fold cross validation analysis was performed using $cAPD_{90}$ threshold (reduction) values. The r^2 value was 0.90 with an RMSE of $Log_{10} = 0.59$, which translates to an error of 3.9-fold. Hence, for compounds with predominant calcium channel antagonism pharmacology there is a clear predictive relationship with corrected APD_{90} threshold values that follows the linear equation of $y = 1.021x + 0.932$.

4. Discussion

The utility of hIPSC-CM's in addressing cardiac risk in preclinical development has been the subject of multiple studies over recent years. These efforts have focused on two main areas, arrhythmogenesis and cardiac contractility. Cardiac arrhythmias arise due to changes in cardiac conduction and/or repolarization and can be induced by ion channel block. Indeed, it is well known that hERG potassium channel inhibition results in a reduced rate of repolarization of the cardiomyocyte resulting in a prolongation of APD that can lead to a potentially life threatening arrythmia, TdP.

Although hERG profiling is now routine in the development of drug candidates, there is growing interest, driven in part by the FDA supported CiPA project, to develop more integrated and humanized cardiac models that include other channels/targets that play a role in the morphology of the cardiac AP (CiPAproject.org; (Colatsky et al., 2016; Fermini et al., 2016). Moreover, the value of hIPSC-CM's has been recognized in recent discussion around the updating of ICH S7B regulatory guidelines (Anon, 2020).

For a hIPSC-CM assay to be valuable in risk assessment there are several criteria the model should address. The model endpoints must show robust clinical translation. Ideally, the assay should be simple, robust, and amenable to high throughput screening to allow profiling of larger compound sets. Moreover, serum-free conditions are key to avoiding potential issues related to compound protein binding. Finally, the ability to measure effects over a more chronic time course is helpful for compounds that have slow on-rates kinetics, or that may affect channel expression.

The expression profile of targets involved in generating the AP in the model is also a consideration. Although human derived, one cannot assume that hIPSC-CM cells have the same expression profile and phenotypic maturity of human adult ventricular cardiomyocytes. Indeed, hIPSC-CM do exhibit an immature electrophysiological phenotype (Garg et al., 2018). In the present study, we examined the expression of genes involved in AP generation. hERG, $Ca_v1.2$ and $Na_v1.5$ were expressed at similar levels compared to purified human ventricular cardiomyocytes. These data are not in agreement with several studies where $Ca_v1.2$ expression was found to be higher and $Na_v1.5$ expression lower in iCell cardiomyocytes compared to human heart tissue (Blinova et al., 2017; Goodrow et al., 2018; Huo et al., 2017).

The present study focused on the ability of hIPSC-CM's to predict multiple clinical endpoints, primarily QTc and QRS intervals of the ECG, together with TdP risk. Although previous studies have focused on predicting TdP risk using hIPSC-CM's, there have been no extensive studies using hIPSC-CM's to define their ability to predict compound-mediated changes in clinical QTc and QRS intervals.

Given the relationship between the QTc interval and APD, we profiled a set of compounds to define the concentration required to produce a threshold increase in APD_{90}. Values were correlated with the free clinical exposure producing a 10 ms increase in QTc. A robust correlation was observed that was not enhanced using rate-corrected values. The linearity of the correlation allows the prediction of the clinical exposures that would produce a 10 ms increase in QTc from hIPSC-CM data using the equation shown in Table 2. Interestingly, given the diverse compound set used in this study, the hERG binding assay was slightly better at predicting QTc. Moreover, a comparison of the larger compound set, where not all compounds had published clinical QTc data, showed a robust correlation of the APD_{90} positive threshold concentration with the hERG binding K_i value, similar to previously reported findings for hERG patch (Saxena et al., 2017).

The ability of a compound to inhibit the hERG channel is closely linked to QTc prolongation and in turn to an increased risk of TdP (Roden, 2004). However, hERG inhibition alone is not the sole determinant of TdP liability. Calcium channel block or late sodium current block can offset a hERG-induced APD prolongation and as such compounds with mixed-ion channel effects may not be associated with an increase in QTc or TdP risk. Therefore, predicting TdP using hERG alone may be challenging and a system that integrates a compounds broader pharmacology may be more predictive.

In this study we selected a diverse compound set with defined TdP risk and used the data from both our hIPSC-CM model, as well as ion channel data, and employed a variety of statistical models/analyses to determine assay endpoints that predicted TdP risk.

Several studies focused on TdP have either relied upon small compound sets, literature ion channel data or data generated from cross-site consortia utilizing multiple methodologies. An advantage of the current study is the use of a single profiling platform to examine an extensive and diverse compound set. In addition, the use of serum free conditions avoids issues associated with changes in free drug levels due to protein binding. Indeed, Blinova et al. (2018) noted significant differences in results from one group in their cross-site study that used serum free conditions, with the authors suggested that this may reflect protein binding. Finally, our model provides the opportunity to examine drug effects over extended time periods, something that has not been examined using an extensive compound set. Extended incubations ensure that responses from compounds with slow onset kinetics or compounds that affected surface ion channel expression are accurately captured.

In general, analyses using endpoints extracted from the hIPSC-CM model were shown to be highly predictive. Results were comparable with previous studies using smaller compound sets and lower throughput assays (Ando et al., 2017; Blinova et al., 2018; Kanda et al., 2018). The hIPSC-CM model was more predictive than either ion channel data alone, O'Hara-Rudy modeling using ion channel data, or a combination of hIPSC-CM data and ion channel data.

Several compounds were misassigned by our model with respect to the TdP risk category (Fig. 3e). These differed from those observed in a recent cross-site study (Blinova et al., 2018) with the exception of ranolazine, which was misassigned as TdP positive in both studies. Ranolazine blockade of late $Na_v1.5$ current counteracts its inhibition of hERG, minimizing its torsadogenic liability. Compared to adult ventricular cardiomyocytes, iPSC-CM's are reported to have a reduced late $Na_v1.5$ current density (Goodrow et al., 2018). As mentioned above, we found no difference in $Na_v1.5$ expression in $iCell^2$ versus adult human cardiomyocytes (Fig. 1), suggesting a reduction in late $Na_v1.5$ current in iPSC-CM's may occur through mechanisms unrelated to expression. Goodrow et al. (2018) have shown that, compared to adult cardiomyocytes, iPSC-CM's have a depolarized $V_{1/2\ (activation)}$ and a hyperpolarized $V_{1/2\ (inactivation)}$. Reducing late $Na_v1.5$ current decreasing the window current could attenuate the AP duration-modifying effects of ranolazine, allowing its inhibition of hERG to predominate and thus generating a TdP positive signal in our model.

With respect to ICH S7B there are two required assessments for molecules entering clinical development. A compound might be considered positive in both (an S7B double positive) or negative in both (a double negative) or have mixed results. The predictive power of the double negative was discussed recently (Strauss et al., 2021; Vargas et al., 2021). The double positive is also informative. Table 4 illustrates the post-test probabilities for the double positive, double negative and two mixed results based on the data presented by Vargas and colleagues (Vargas et al., 2021). The two double results are sufficiently informative to facilitate decision-making for most compounds. The mixed results having post-test probabilities of 4.7% and 22% may require follow-up. Applying the hIPSC-CM model to these compounds would contribute to an overall weight of evidence regarding TdP liability. Alternative flow

schemes such as hERG patch followed by hIPSC-CM then in vivo QTc might also be considered depending on the individuals desire to optimize positive or negative predictive power versus time and cost using this Bayesian methodology (Felli and Leishman, 2020).

With respect to translation of compound-mediated changes in clinical QRS there have been a number of studies that utilize either small compound sets or compare data to preclinical in vivo endpoints (Harris et al., 2013), but no extensive studies comparing a hIPSC-CM model to clinical data. The AP rise-time endpoint is largely driven by the $Na_v1.5$ current. An ROC cross validation analysis of AP rise-time versus the ability of compounds to produce an increase in clinical QRS interval showed excellent predictivity that was greater than that using $Na_v1.5$ patch data, highlighting the value of this model in assessing QRS risk.

This study has several potential limitations. Firstly, hIPSC-CM's do not show a mature cardiomyocyte phenotype. In our hands iCell^2 produce the characteristic negative inotropic response when treated with positive inotropes that is a hallmark of such an immature phenotype. However, the cells do appear to provide a robust predictive model of QTc and QRS changes as well as TdP and as such appear fit for purpose. Second, TdP analyses rely heavily on the accuracy of the TdP clinical risk definitions for each compound. This categorization can be challenging due to the low incidence rate, hence if not accurate this will affect the overall prediction of any potential model.

In summary, we describe a hIPSC-CM model that can predict clinic QTc, QRS and TdP risk. The high throughput format and serum-free conditions provide additional advantages in profiling early development compounds. In addition, the ability to run the assay over extended incubation times allows the characterization of compounds with slow on-rate kinetics or that affect channel trafficking, that would be missed using acute assays. Moreover, this assay replaces the need for ex vivo animal models, such as the Langendorff isolated heart model, that are routinely used to assess such risks. As such this model will play a key role in the early assessment of cardiac safety of development compounds.

Data availability statement

Additional supporting data may be found online in the Supporting Information section.

Funding

This research did not receive any specific grant from funding agencies in the public, commercial, or not-for-profit sectors.

CRediT authorship contribution statement

Peter Kilfoil: Formal analysis, Investigation, Methodology, Writing – original draft. **Shuyun Lily Feng:** Formal analysis, Investigation, Methodology. **Asser Bassyouni:** Formal analysis, Investigation, Methodology, Writing – review & editing. **Tiffany Lee:** Formal analysis, Investigation, Writing – review & editing. **Derek Leishman:** Formal analysis, Writing – review & editing. **Dingzhou Li:** Formal analysis, Writing – review & editing. **David J. MacEwan:** Writing – review & editing. **Parveen Sharma:** Writing – review & editing. **Eric D. Watt:** Data curation, Formal analysis, Software, Methodology, Writing – original draft, Visualization. **Stephen Jenkinson:** Conceptualization, Data curation, Formal analysis, Investigation, Methodology, Writing – original draft, Visualization, Supervision.

Declaration of competing interest

The authors declare that they have no known competing financial interests or personal relationships that could have appeared to influence the work reported in this paper.

Acknowledgements

This work was supported by Pfizer Inc. The authors would like to thank Todd Wisialowski and Gregg Cappon for their critical review of this manuscript and their insightful suggestions.

Appendix A. Supplementary data

Supplementary data to this article can be found online at https://doi.org/10.1016/j.ejphar.2021.174584.

References

Akaike, H., 1998. Information theory and an extension of the maximum likelihood principle. In: Parzen, E., Tanabe, K., Kitagawa, G. (Eds.), Selected Papers of Hirotugu Akaike. Springer, New York, NY, pp. 199–213.

Ando, H., Yoshinaga, T., Yamamoto, W., Asakura, K., Uda, T., Taniguchi, T., et al., 2017. A new paradigm for drug-induced torsadogenic risk assessment using human iPS cell-derived cardiomyocytes. J. Pharmacol. Toxicol. Methods 84, 111–127.

Anon, 2020. E14 and S7B clinical and nonclinical evaluation of QT/QTc interval prolongation and proarrhythmic potential - questions and answers. Retrieved from. https://www.fda.gov/regulatory-information/search-fda-guidance-documents/e14-and-s7b-clinical-and-nonclinical-evaluation-qtqtc-interval-prolongation-and-proarrhythmic.

Bazett, H.C., 1920. An analysis of the time-relations of the electrocardiograms. Heart 7, 353–370.

Blinova, K., Dang, Q., Millard, D., Smith, G., Pierson, J., Guo, L., et al., 2018. International multisite study of human-induced pluripotent stem cell-derived cardiomyocytes for drug proarrhythmic potential assessment. Cell Rep. 24, 3582–3592.

Blinova, K., Stohlman, J., Vicente, J., Chan, D., Johannesen, L., Hortigon-Vinagre, M.P., et al., 2017. Comprehensive translational assessment of human-induced pluripotent stem cell derived cardiomyocytes for evaluating drug-induced arrhythmias. Toxicol. Sci. 155, 234–247.

Colatsky, T., Fermini, B., Gintant, G., Pierson, J.B., Sager, P., Sekino, Y., et al., 2016. The comprehensive in vitro Proarrhythmia assay (CiPA) initiative - update on progress. J. Pharmacol. Toxicol. Methods 81, 15–20.

Felli, J.C., Leishman, D.J., 2020. A Bayesian approach to toxicological testing. J. Pharmacol. Toxicol. Methods 105, 106898.

Fermini, B., Hancox, J.C., Abi-Gerges, N., Bridgland-Taylor, M., Chaudhary, K.W., Colatsky, T., et al., 2016. A new perspective in the field of cardiac safety testing through the comprehensive in vitro Proarrhythmia assay paradigm. J. Biomol. Screen 21, 1–11.

Ficker, E., Dennis, A.T., Wang, L., Brown, A.M., 2003. Role of the cytosolic chaperones Hsp70 and Hsp90 in maturation of the cardiac potassium channel HERG. Circ. Res. 92, e87–100.

Filer, D.L., Kothiya, P., Setzer, R.W., Judson, R.S., Martin, M.T., 2017. tcpl: the ToxCast pipeline for high-throughput screening data. Bioinformatics 33, 618–620.

Food, & Drug Administration HHS, 2005. International conference on harmonisation; guidance on S7B nonclinical evaluation of the potential for delayed ventricular repolarization (QT interval prolongation) by human pharmaceuticals; availability. Notice. Fed. Regist. 70, 61133–61134.

Fridericia, L.S., 1920. Die systolendauer im elektrokardiogramm bei normalen menschen und bei herzkranken. Acta Med. Scand. 53, 469–486.

Friedman, J., Hastie, T., Tibshirani, R., 2010. Regularization paths for generalized linear models via coordinate descent. J. Stat. Software 33, 1–22.

Garg, P., Garg, V., Shrestha, R., Sanguinetti, M.C., Kamp, T.J., Wu, J.C., 2018. Human induced pluripotent stem cell-derived cardiomyocytes as models for cardiac channelopathies: a primer for non-electrophysiologists. Circ. Res. 123, 224–243.

Gintant, G., Fermini, B., Stockbridge, N., Strauss, D., 2017. The evolving roles of human iPSC-derived cardiomyocytes in drug safety and discovery. Cell Stem Cell 21, 14–17.

Gintant, G., Kaushik, E.P., Feaster, T., Stoelzle-Feix, S., Kanda, Y., Osada, T., et al., 2020. Repolarization studies using human stem cell-derived cardiomyocytes: validation studies and best practice recommendations. Regul. Toxicol. Pharmacol. 117, 104756.

Gintant, G., Traebert, M., 2020. The roles of human induced pluripotent stem cell-derived cardiomyocytes in drug discovery: managing in vitro safety study expectations. Expet Opin. Drug Discov. 15, 719–729.

Goksuluk, D., Krokmaz, S., Zararsiz, G., Karaagaoglu, A.E., 2016. An interactive web-tool for ROC curve analysis using R language environment. R J. 8, 213–230.

Goodrow Jr., R.J., Desai, S., Treat, J.A., Panama, B.K., Desai, M., Nesterenko, V.V., et al., 2018. Biophysical comparison of sodium currents in native cardiac myocytes and human induced pluripotent stem cell-derived cardiomyocytes. J. Pharmacol. Toxicol. Methods 90, 19–30.

Harmer, A.R., Valentin, J.P., Pollard, C.E., 2011. On the relationship between block of the cardiac Na(+) channel and drug-induced prolongation of the QRS complex. Br. J. Pharmacol. 164, 260–273.

Harris, K., Aylott, M., Cui, Y., Louttit, J.B., McMahon, N.C., Sridhar, A., 2013. Comparison of electrophysiological data from human-induced pluripotent stem cell-derived cardiomyocytes to functional preclinical safety assays. Toxicol. Sci. 134, 412–426.

Huang, Y.L., Walker, A.S., Miller, E.W., 2015. A photostable silicon rhodamine platform for optical voltage sensing. J. Am. Chem. Soc. 137, 10767–10776.
Huo, J., Kamalakar, A., Yang, X., Word, B., Stockbridge, N., Lyn-Cook, B., et al., 2017. Evaluation of batch variations in induced pluripotent stem cell-derived human cardiomyocytes from 2 major suppliers. Toxicol. Sci. 156, 25–38.
Ivashchenko, C.Y., Pipes, G.C., Lozinskaya, I.M., Lin, Z., Xiaoping, X., Needle, S., et al., 2013. Human-induced pluripotent stem cell-derived cardiomyocytes exhibit temporal changes in phenotype. Am. J. Physiol. Heart Circ. Physiol. 305, H913–H922.
Johannesen, L., Vicente, J., Mason, J.W., Sanabria, C., Waite-Labott, K., Hong, M., et al., 2014. Differentiating drug-induced multichannel block on the electrocardiogram: randomized study of dofetilide, quinidine, ranolazine, and verapamil. Clin. Pharmacol. Ther. 96, 549–558.
Johnson, S.G., 2017. The NLopt nonlinear-optimization package. Retrieved from. http://github.com/stevengj/nlopt.
Kanda, Y., Yamazaki, D., Osada, T., Yoshinaga, T., Sawada, K., 2018. Development of torsadogenic risk assessment using human induced pluripotent stem cell-derived cardiomyocytes: Japan iPS Cardiac Safety Assessment (JiCSA) update. J. Pharmacol. Sci. 138, 233–239.
Kuhn, M., 2020. Caret: Classification and Regression Training. Retrieved from. https://CRAN.R-project.org/package=caret.
Lancaster, M.C., Sobie, E.A., 2016. Improved prediction of drug-induced Torsades de Pointes through simulations of Dynamics and machine learning algorithms. Clin. Pharmacol. Ther. 100, 371–379.
Lee, H.A., Hyun, S.A., Park, S.G., Kim, K.S., Kim, S.J., 2016. Comparison of electrophysiological effects of calcium channel blockers on cardiac repolarization. KOREAN J. PHYSIOL. PHARMACOL. 20, 119–127.
Liaw, A., Wiener, M., 2002. Classification and regression by randomForest. R. News 2, 18–22.
Ma, J., Guo, L., Fiene, S.J., Anson, B.D., Thomson, J.A., Kamp, T.J., et al., 2011. High purity human-induced pluripotent stem cell-derived cardiomyocytes: electrophysiological properties of action potentials and ionic currents. Am. J. Physiol. Heart Circ. Physiol. 301, H2006–H2017.
Matthews, B.W., 1975. Comparison of the predicted and observed secondary structure of T4 phage lysozyme. Biochim. Biophys. Acta 405, 442–451.
Millard, D., Dang, Q., Shi, H., Zhang, X., Strock, C., Kraushaar, U., et al., 2018. Cross-site reliability of human induced pluripotent stem cell-derived cardiomyocyte based safety assays using microelectrode arrays: results from a blinded CiPA pilot study. Toxicol. Sci. 164, 550–562.
Nguyen, N., Nguyen, W., Nguyenton, B., Ratchada, P., Page, G., Miller, P.E., et al., 2017. Adult human primary cardiomyocyte-based model for the simultaneous prediction of drug-induced inotropic and pro-arrhythmia risk. Front. Physiol. 8, 1073.
O'Hara, T., Virag, L., Varro, A., Rudy, Y., 2011. Simulation of the undiseased human cardiac ventricular action potential: model formulation and experimental validation. PLoS Comput. Biol. 7, e1002061.
Page, G., Ratchada, P., Miron, Y., Steiner, G., Ghetti, A., Miller, P.E., et al., 2016. Human ex-vivo action potential model for pro-arrhythmia risk assessment. J. Pharmacol. Toxicol. Methods 81, 183–195.
Pfeiffer-Kaushik, E.R., Smith, G.L., Cai, B., Dempsey, G.T., Hortigon-Vinagre, M.P., Zamora, V., et al., 2019. Electrophysiological characterization of drug response in hSC-derived cardiomyocytes using voltage-sensitive optical platforms. J. Pharmacol. Toxicol. Methods 99, 106612.
Powell Mjd, 2009. The BOBYQA Algorithm for Bound Constrained Optimization without Derivatives. Retrieved from. http://www.damtp.cam.ac.uk/user/na/NA_papers/NA2009_06.pdf.
R-Project, 2019. R: A Language and Environment for Statistical Computing. Retrieved from. https://www.R-project.org/.
Ribeiro, A.J.S., Guth, B.D., Engwall, M., Eldridge, S., Foley, C.M., Guo, L., et al., 2019. Considerations for an in vitro, cell-based testing platform for detection of drug-induced inotropic effects in early drug development. Part 2: designing and fabricating microsystems for assaying cardiac contractility with physiological relevance using human iPSC-cardiomyocytes. Front. Pharmacol. 10, 934.
Roden, D.M., 2004. Drug-induced prolongation of the QT interval. N. Engl. J. Med. 350, 1013–1022.
Saxena, P., Hortigon-Vinagre, M.P., Beyl, S., Baburin, I., Andranovits, S., Iqbal, S.M., et al., 2017. Correlation between human ether-a-go-go-related gene channel inhibition and action potential prolongation. Br. J. Pharmacol. 174, 3081–3093.
Spearman, C., 1987. The proof and measurement of association between two things. By C. Spearman, 1904. Am. J. Psychol. 100, 441–471.
Strauss, D.G., Wu, W.W., Li, Z., Koerner, J., Garnett, C., 2021. Translational models and tools to reduce clinical trials and improve regulatory decision making for QTc and Proarrhythmia risk (ICH E14/S7B updates). Clin. Pharmacol. Ther. 109, 319–333.
Tan, H.L., Bezzina, C.R., Smits, J.P., Verkerk, A.O., Wilde, A.A., 2003. Genetic control of sodium channel function. Cardiovasc. Res. 57, 961–973.
Therneau, T., Atkinson, B., 2019. Rpart: recursive partitioning and regression trees. Retreived from. https://CRAN.R-project.org/package=rpart.
Vargas, H.M., Rolf, M.G., Wisialowski, T.A., Achanzar, W., Bahinski, A., Bass, A., et al., 2021. Time for a fully integrated nonclinical-clinical risk assessment to streamline QT prolongation liability determinations: a pharma industry perspective. Clin. Pharmacol. Ther. 109, 310–318.
Welch, B.L., 1947. The generalisation of student's problems when several different population variances are involved. Biometrika 34, 28–35.
Yamamoto, W., Asakura, K., Ando, H., Taniguchi, T., Ojima, A., Uda, T., et al., 2016. Electrophysiological characteristics of human iPSC-derived cardiomyocytes for the assessment of drug-induced proarrhythmic potential. PLoS One 11, e0167348.
Zeng, H., Wang, J., Clouse, H., Lagrutta, A., Sannajust, F., 2019. Resolving the reversed rate effect of calcium channel blockers on human-induced pluripotent stem cell-derived cardiomyocytes and the impact on in vitro cardiac safety evaluation. Toxicol. Sci. 167, 573–580.
Zhao, Z., Lan, H., El-Battrawy, I., Li, X., Buljubasic, F., Sattler, K., et al., 2018. ion channel expression and characterization in human induced pluripotent stem cell-derived cardiomyocytes. Stem Cell. Int. 2018, 6067096.
Zhu, W.Z., Santana, L.F., Laflamme, M.A., 2009. Local control of excitation-contraction coupling in human embryonic stem cell-derived cardiomyocytes. PLoS One 4, e5407.